Published by Institute of Physics Publishing for SISSA

Received: *April 11, 2005*
Accepted: *May 30, 2005*
Published: *June 28, 2005*

Cosmic ray signals from mini black holes in models with extra dimensions: an analytical/Monte Carlo study

Alessandro Cafarella and Claudio Corianò

Dipartimento di Fisica, Università di Lecce and
I.N.F.N. Sezione di Lecce
Via Arnesano, 73100 Lecce, Italy
E-mail: Alessandro.Cafarella@le.infn.it, Claudio.Coriano@le.infn.it

Theodore N. Tomaras

Department of Physics and Institute for Plasma Physics
University of Crete and FO.R.T.H.
Heraklion, Crete, Hellas
E-mail: tomaras@physics.uoc.gr

Abstract: It is shown that the partial and total multiplicities and the lateral distributions of the shower particles can distinguish between events produced by the evaporation of mini black holes from normal ones with the same energy due, for instance, to a primary-proton - nucleon collision. The analysis is performed via a large scale simulation of the resulting cascades in the two cases over the entire range ($10^{15} - 10^{19}$ eV) of ultra high energies, for several values of the number of large extra dimensions, for a variety of altitudes of the initial interaction and with the energy losses in the bulk taken into account. The electromagnetic/hadronic ratio is strongly fluctuating and, thus, not conclusive for the altitudes considered. The relevance of these results to a possible black hole interpretation of the Centauro events is commented upon.

Keywords: Large Extra Dimensions, D-branes, Black Holes, High Energy Cosmic Rays.

Contents

1. Introduction

In the context of a Brane-World model with TeV-scale gravity and large compact or non-compact extra dimensions [1] it is reasonable to expect that mini black holes, black holes with mass a few TeV, can form by the impact of ultra high energy primary cosmic rays with nucleons in the atmosphere [2–4]. Such a black hole is expected to evaporate instantly into all types of particles of the Standard Model and gravity. The initial partons will hadronize and all resulting particles as they propagate in the atmosphere will develop into a shower(s), which eventually will reach the detectors. How do these showers look like, what are their characteristics and how are they different from the usual ones, not due to evaporating mini black holes but to ordinary parton - parton collisions in the atmosphere? No such quantitative comparative study has been performed so far and the present article is a first step in this direction.

It will be shown that the partial and total multiplicities, as well as the lateral distributions of the showers are indeed very different in black hole mediated events and normal events and can serve to distinguish them. As a byproduct, our results lend quantitative support to the recently proposed evaporating mini black hole interpretation [5, 6] of the Centauros [7].

Clearly, the problem of evaporation of a mini black hole in the framework of a D-brane world model, the fragmentation and hadronization of the partons produced, cannot at this stage be attacked in full generality. To procceed we shall rely on the following simplifying assumptions and approximations: (1) The brane tension is taken much smaller than the fundamental gravity scale, so it does not modify the flat background metric. (2) The black hole, somehow produced [5], is assumed to immediately get rid of its "hair" and spin and then evaporate instantly (the "sudden approximation") leading to initial "partons", whose number and distributions are obtained semiclassically. No virtual holes are discussed and no back reaction is taken into account. (3) The initial decay products are assumed to fly away in an s-wave and hadronize, with no intermediate formation of a quark-gluon plasma or of a disoriented chiral condensate (DCC).

To investigate the detailed nature of the air showers produced, we use the Monte Carlo simulation program CORSIKA [8, 9], with the hadronic interaction implemented in SIBYLL [10], in order to perform this comparison, selecting a benchmark process which can be realistically simulated by this Monte Carlo. Finally, since the multiplicities and lateral distributions of the showers produced at a given energy do not depend on the direction of motion of the intermediate black hole, we decided, with no loss of generality, to concentrate on simulations of ultra high energy cosmic ray showers coming, just like the Centauros, down vertically towards the detectors.

The present paper consists of six sections, of which this Introduction is the first. In Section 2 we briefly describe the D-brane world scenario, in order to state clearly the fundamental theoretical assumptions in our study. The basic properties of mini black holes, useful semiclassical formulae, as well as the details of our modeling of the black hole radiation emission, are reviewed here. Section 3 contains our modeling of the hadronization process. The hadronization of the partons emitted by the black hole is treated analytically in the black hole rest frame, by solving the evolution equations for the parton fragmentation functions, making use of a special algorithm [11] and of a specific set of initial conditions for these functions [12]. After a brief discussion in section 4 of the transformation of the kinematics of the black hole decay event from the black hole frame to the laboratory frame, we proceed in Section 5 with the Monte Carlo simulation of the air showers of the particles produced by taking these particles as primaries. The simulations are quite intensive and have been performed on a small computer cluster. As we have already mentioned, in this work we focus mainly on the multiplicities and on the lateral distributions of the events and scan the entire ultra high energy part of the cosmic ray spectrum. Our results are summarized in a series of plots and are commented upon in the final discussion section 6.

2. TeV scale gravity, large extra dimensions and mini black holes

The theoretical framework of the present study is the D-brane world scenario [1]. The World according to this scenario is 10 dimensional, but all the Standard Model matter and forces are confined on a $4 + n_L$ dimensional hypersurface (the D_{3+n_L}-brane). Only gravity with a characteristic scale M_* can propagate in the bulk. The n_L longitudinal dimensions are constrained experimentally to be smaller than $\mathcal{O}\,(TeV^{-1})$. However, for our purposes these dimensions may be neglected, since the Kaluza-Klein excitations related to these have masses a few TeV, too large to affect considerably our discussion below. Consistency with the observed Newton's law, on the other hand, leads to the relation $M_{Pl}^2 = M_*^{n+2} V_n$, between $M_{Pl} \simeq 10^{19}\,\mathrm{GeV}$, the fundamental gravity scale M_* and the volume V_n of the $n = 6 - n_L$ dimensional compact or non-compact transverse space. A natural choice for M_*, dictated a priori by the "gauge hierarchy" puzzle, is $M_* \simeq \mathcal{O}(M_W) \simeq \mathcal{O}(1\,\mathrm{TeV})$, while the simplest choice for the transverse space is an n-dimensional torus with all radii equal to R. Thus, one obtains a condition between the number n and the size $R(n)$ of the transverse dimensions. Notice that under the above assumptions and for all values of n, R is much larger than 10^{-33}cm, the length scale at which one traditionally expects possible deviations from the 3-dimensional gravity force, and the corresponding dimensions are termed "large extra dimensions" (LED). For $n = 2$ one obtains $R(n = 2)$ of the order of a fraction of a mm. At distances much smaller than R one should observe $3+n$-dimensional Newton's law. Current bounds on the size of these large extra dimensions and on M_* come from various arguments, mostly of astrophysical (for instance $M_* > 1500\,\mathrm{TeV}$ for $n = 2$) or cosmological ($M_* > 1.5\,\mathrm{TeV}$ for $n = 4$) origin [13]. A larger number of LED (n) translates into a reduced lower bound on M_*. It should be pointed out, that in general it is possible, even if "unatural", that the transverse space has a few dimensions large and the others small. Here we shall assume a value of M_* of order 1 TeV, neglect the small extra dimensions and treat the number of LED (n) as a free parameter.

The implications of the existence of LED are quite direct in the case of black hole physics. The black hole is effectively 4-dimensional if its horizon (r_H) is larger than the size of the extra dimensions. In the opposite case ($r_H \ll R$, or equivalently for black hole masses $M_{BH} \ll 10^{13}$kg for $n = 6$ [5]) it is $4 + n$ dimensional, it spreads over the full space and its properties are those of a genuine higher dimensional hole. According to some estimates, over which however there is no universal consensus [14], black holes should be produced copiously [2]–[4] in particle collisions, whenever the center of mass energy available in the collision is considerably larger than the effective scale M_* ($\sqrt{s} \gg M_*$). With $M_* \sim 1\,\mathrm{TeV}$, one may contemplate the possibility of producing black holes with masses of order a few TeV.

As mentioned in the introduction, we shall use the results of the semiclassical study of the black hole radiation only in its Schwarzschild phase, during which it is described by the metric of the $4 + n$ dimensional black hole

$$ds^2 = \left[1 - \left(\frac{r_H}{r}\right)^{n+1}\right] dt^2 - \left[1 - \left(\frac{r_H}{r}\right)^{n+1}\right]^{-1} dr^2 - r^2 d\Omega^2_{2+n}\,, \tag{2.1}$$

where n denotes the number of extra spacelike dimensions, and $d\Omega^2_{2+n}$ is the line element of the $(2+n)$-dimensional unit sphere. The temperature T_H of the black hole [15] is related to the size of its horizon by [16]

$$T_H = \frac{n+1}{4\pi\, r_H} \tag{2.2}$$

and the formula for the horizon r_H can be expressed in terms of the mass of the black hole M_{BH} and the gravity scale M_* [16]

$$r_H = \frac{1}{\sqrt{\pi} M_*} \left(\frac{M_{BH}}{M_*}\right)^{\frac{1}{n+1}} \left(\frac{8\Gamma\left(\frac{n+3}{2}\right)}{n+2}\right)^{\frac{1}{n+1}} . \tag{2.3}$$

For $n = 0$ and $M_* = M_{Pl} = G^{-1/2} \simeq 10^{19}\,\mathrm{GeV}$ it reproduces the usual formula for the horizon ($r_H = 2GM_{BH}$) of a 4 dimensional black hole. For $n > 0$ the relation between r_H and M_{BH} becomes nonlinear and the presence of M_* in the denominator of eq. (2.3) in place of M_{Pl} increases the horizon size for a given M_{BH}. For $M_{BH}/M_* \sim 5$ and $M_* = 1\,\mathrm{TeV}$ the size of the horizon is around 10^{-4} fm and decreases with increasing n.

JHEP06(2005)065

In the Schwarzschild phase, the number of particles emitted per unit time by the black hole as a function of energy is expressed in terms of the absorption/emission cross sections $\sigma^{(s)}_{j,n}(\omega)$ (or equivalently of the greybody factors $\Gamma(\omega)$), which, apart from n, depend on the spin (s) of the emitted particle, the angular momentum (j) of the partial wave and the corresponding energy (ω),

$$\frac{dN^{(s)}(\omega)}{dtd\omega} = \sum_j \frac{\sigma^{(s)}_{j,n}(\omega)}{2\pi^2} \frac{\omega^2}{\exp\left(\omega/T_H\right) \pm 1} . \tag{2.4}$$

where the sum is over all Standard Model particles and the $+(-)$ in the denominator corresponds to fermions (bosons), respectively. $\sigma^{(s)}_{j,n}$ are the cross sections for the various partial waves and depend on the spin s of each particle. Multiplying the rate of emitted particles per energy interval $dN^{(s)}(\omega)/dtd\omega$ by the particle energy ω one obtains for the power emission density $dE^{(s)}(\omega)/dtd\omega = \omega dN^{(s)}(\omega)/dtd\omega$.

We recall, that in the geometric optics approximation a black hole acts as a perfect absorber of slightly larger than r_H radius r_c [17], defined as the critical radius for null geodesics

$$r_c = \left(\frac{n+3}{2}\right)^{1/(n+1)} \sqrt{\frac{n+3}{n+1}} r_H . \tag{2.5}$$

The optical cross section is then defined in terms of r_c (or equivalently r_H via eq. (2.5)), such that A_k, the effective surface area of the black hole projected over a k-dimensional sub-manifold becomes [18]:

$$A_k = \Omega_{k-2} \left(\frac{d-1}{2}\right)^{\frac{2}{d-3}} \left(\frac{d-1}{d-3}\right)^{\frac{k-2}{2}} r_H^{k-2} \tag{2.6}$$

and $\Omega_k = 2\pi^{\frac{k+1}{2}}/\Gamma(\frac{k+1}{2})$ is the volume of a k-sphere with unit radius. It is convenient to rewrite the greybody factors as a dimensionless constant $\Gamma_s = \sigma_s/A_4$ normalized to the effective area of the horizon A_4, obtained from (2.6) for $k=4$ and $d=4+n$

$$A_4 = 4\pi \left(\frac{n+3}{2}\right)^{2/(n+1)} \frac{n+3}{n+1} r_H^2 , \tag{2.7}$$

and replacing the particle cross section σ in terms of a thermal averaged greybody factor $\Gamma_i(\Gamma_{1/2} = 2/3, \Gamma_1 = 1/4, \Gamma_0 = 1$, i denoting the spin or species [19]). Eqs. (2.4) integrated over the frequency give (for particle i)

$$\frac{dN_i}{dt} = \alpha(n, r_H)\, T_H^3 \tag{2.8}$$

with

$$\alpha(n, r_H) = \frac{f_i}{2\pi^2}\, \Gamma_i\, \Gamma(3)\, \zeta(3)\, c_i\, A_4\, T_H^3 , \tag{2.9}$$

where c_i is the number of degrees of freedom of particle i and f_i is defined by the integral (s_i is the spin)

$$\int_0^\infty d\,\omega \frac{\omega^2}{e^{\omega/T_H} - (-1)^{2s_i}} = f_i\, \Gamma(3)\, \zeta(3)\, T_H^3 \tag{2.10}$$

from which $f_i = 1$ ($f_i = 3/4$) for bosons (fermions). These numbers depend on the dimension of the brane, which in our case is 3. $\Gamma(x)$ and $\zeta(x)$ are the Gamma and the Riemann function respectively. Using (2.7) and (2.2), equation (2.8) becomes

$$\frac{dN_i}{dt} = \frac{f_i}{8\pi^3}\frac{(n+3)^{(n+3)/(n+1)}}{2^{2/(n+1)}}(n+1)\Gamma(3)\zeta(3)\Gamma_i c_i T_H. \tag{2.11}$$

and upon summation over all species i

$$\frac{dN}{dt} = \frac{1}{2\pi}\left(\sum_i f_i\,\overline{\Gamma}_i\,c_i\right)\Gamma(3)\,\zeta(3)\,T_H \tag{2.12}$$

where

$$\overline{\Gamma}_i = \frac{\Gamma_i(n+1)\,(n+3)^{(n+3)/(n+1)}}{4\pi^2\,2^{2/(n+1)}}. \tag{2.13}$$

The resulting emission rates are given by

$$\dot{N}_i \approx 4\times 3.7\times 10^{21}\,\frac{(n+3)^{(n+3)/(n+1)}(n+1)}{2^{2/(n+1)}}\left(\frac{T_H}{\mathrm{GeV}}\right)\,\mathrm{s}^{-1}\,, \tag{2.14}$$

for particles with $s = 0$ and $1/2$, while for $s = 1$ the rate is reduced by a factor of 20.

Furthermore, integration of $dE^{(s)}(\omega)/dtd\omega$ over ω gives for the black hole mass evolution

$$\frac{dM}{dt} \equiv -\frac{dE}{dt} = \beta(n, r_H)\,T_H^4 = \frac{1}{2\pi}\left(\sum_i f_i\,\overline{\Gamma}_i\,c_i\right)\Gamma(4)\,\zeta(4)\,T_H^2\,, \tag{2.15}$$

with

$$\beta = \frac{1}{2\pi^2}\sum_i\left(c_i\,\Gamma_i\,{f'}_i\right)\,A_4\,\Gamma(4)\,\zeta(4) \tag{2.16}$$

and $f'_i = 1$ (7/8) for bosons (fermions). Taking the ratio of the two equations (2.15) and (2.12) we obtain

$$\frac{dN}{dM} = \left(\frac{\alpha}{\beta}\right)\frac{1}{T_H} = \rho\frac{4\pi\theta(n)}{n+1}\frac{1}{M_*}\left(\frac{M}{M_*}\right)^{\frac{1}{(n+1)}}\,, \tag{2.17}$$

where we have defined

$$\theta(n) = \left(\frac{8\Gamma\left(\frac{n+3}{2}\right)}{n+2}\right)^{\frac{1}{n+1}}\frac{1}{\sqrt{\pi}}\,, \tag{2.18}$$

and

$$\rho = \frac{\sum_i c_i\,f_i\,\Gamma_i\,\Gamma(3)\,\zeta(3)}{\sum_i c_i\,{f'}_i\,\Gamma_i\,\Gamma(4)\,\zeta(4)}\,. \tag{2.19}$$

This formula does not include corrections from emission in the bulk.

In the "sudden approximation", in which the black hole is assumed to decay at its initial formation temperature, one easily finds $N = \left\langle\frac{M_{BH}}{E}\right\rangle$, where E is the energy spectrum of the decay products, and using Boltzmann statistics $N \approx \frac{M_{BH}}{2T_H}$ one obtains the approximate expression [2]

$$N = \frac{2\pi}{n+1}\left(\frac{M_{BH}}{M_*}\right)^{\frac{n+2}{n+1}}\theta(n) = \frac{1}{2}\frac{n+2}{n+1}S_0 \tag{2.20}$$

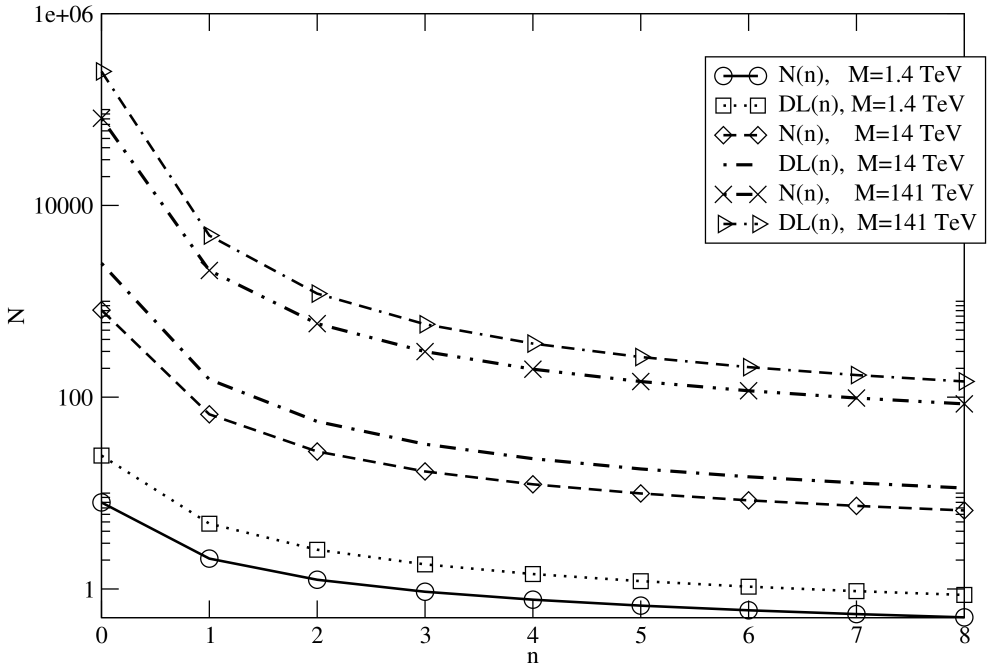

Figure 1: Multiplicities computed with eq. (2.21) (N(n)) and eq. (2.20) (DL(n)) for a varying number of extra dimensions n. DL(n) is the expression given in [2].

in terms of the semiclassical entropy $S_0 = (n+1)M_{BH}/(n+2)T_H$ of the black hole. This formula is certainly adequate for our purposes and the level of theoretical accuracy required at the present stage in cosmic ray physics. However, a more accurate expression is

$$N = \rho \frac{4\pi}{n+2} \left(\frac{M_{BH}}{M_*} \right)^{\frac{n+2}{n+1}} \theta(n) = \rho S_0 \, , \tag{2.21}$$

obtained by integrating (2.17) from zero to M_{BH}. Others may be found in [20]. The above two formulas for the total multiplicity are plotted in figure 1 for varying n and M_{BH}. As one can see, the two formulas are quite close, as expected, but eq. (2.20) gives larger values for the multiplicities compared to (2.21) as noted in [21].

Overall, in the massless approximation, the mini black hole decay products for a 3-brane consist of approximately 2% spin zero, 85% spin half and 13% spin one particles, with similar contributions also to the power emissivities. These numbers change as we vary the dimension of the brane (d) and so does the formula for the emissivities, since the number of brane degrees of freedom ($c_i(d)$) has to be recomputed, together with the integrals on the emission spectra ($f_i(d)$) [22].

The integration of the equation for the power spectrum in the massless approximation can be used to compute the total time of decay (assuming no mass evolution during the decay)

$$\tau \sim \frac{1}{M_*} \left(\frac{M_{BH}}{M_*} \right)^{(n+3)/(n+1)} \tag{2.22}$$

n	0	1	2	3	4
f_n	0.70711	0.66533	0.63894	0.62057	0.60696

Table 1: Fraction f_n of E_{CM} that is bound into the black hole as a function of the number n of extra-dimension in head-on collisions.

which implies that at an energy of approximately 1 TeV the decay time is of the order of 10^{-27} seconds. Therefore strong interaction effects and gravity effects appear to be widely separated and hadronization of the partons takes place after their crossing of the horizon. The black hole is assumed to decay isotropically (s-wave) to a set of N elementary states, selected with equal probability from all the possible states available in the Standard Model.

We shall take into account the (semiclassical) energy loss due to bulk emission in the formation process of the black hole. The energy of the black hole is a fraction f_n (depending on the number of extra dimensions) of the initially available in the center of mass frame of the initial partons and is given by

$$M_{BH} = E_{CM} f_n \tag{2.23}$$

with the numerical values for f_n in head-on collisions reported in table 1 [23].

The energy per partonic channel will be appropriately weighted and we will assume that each parton f will decay into a final state hadron h (carrying a fraction x of the original momentum), with a probability distribution given by the corresponding fragmentation function $D_f^h(x, Q^2)$, which is evolved from some low energy input scale Q_0 up to the relevant scale characterizing the decay. This is given by the available energy per fundamental state, equally distributed among all the states.

The quantification of the injection spectrum involves a computation of the relevant probabilities for the formation of all the possible hadronic/leptonic states prior to the simulation of the air shower. Let us briefly elaborate on this.

To move from the parton level to hadrons, we let $D_q^h(x, Q^2)$, $D_{\overline{q}}^h(x, Q^2)$, and $D_g^h(x, Q^2)$ be the fragmentation functions of N_F quarks q, antiquarks $\overline{q}$, and of the gluon g, respectively, into some hadron h with momentum fraction x at scale Q. From the fragmentation functions we obtain, for each hadron h, the mean multiplicity of the corresponding s-wave and the corresponding average energy and momentum. Specifically, we obtain

$$\langle D_h \rangle = \sum_f \int_{z_{\min}}^1 dz\, D_f^h(z, Q^2) \tag{2.24}$$

for the probability of producing a hadron h, and

$$E_h^* = \sum_f \int_{z_{\min}}^1 z\, dz\, D_f^h(z, Q^2) \tag{2.25}$$

for the average energy of the same hadron. We recall that $z_{\min}$ is the minimal fraction of energy a hadron h, of mass m_h, can take at a scale Q, and can be defined as $z_{\min} = m_h/(Q/2)$. In practical applications one can take the nominal value $z_{\min} = 0.05$ for every hadron, without affecting much the mean multiplicities and the related probabilities. This implies that

$$\langle D_r^h\rangle + \sum_f \langle D_f^h\rangle + \langle D_g^h\rangle + \langle D_\gamma^h\rangle \equiv \mathrm{Pr}_h \tag{2.26}$$

together with the condition $\sum_h \mathrm{Pr}_h = 1$, where the sum runs over all types of hadrons allowed by the fragmentation. In all the equations above, the fragmentation takes place at the typical scale $Q \simeq M_{BH}/N$, scale at which the moments are computed numerically. The relative abundances of the various partons among the initial decay products of the black hole are $p_f = 2 \times 2 \times 3/123$ for each quark flavor except the top (counting spin, particle-antiparticle,[1] and color) $p_g = 2 \times 8/123$ for gluons, $p_\gamma = 2/123$ for the photon. In the remaining states (r) we lump all the states which have been unaccounted for and whose probabilities p_r are computed by difference. These include the top and the antitop (12/123), the W's and Z (9/123) and the leptons (24/123). The fragmentation functions into hadrons, corresponding to these states, $\langle D_r^h\rangle$ are computed by difference from the remaining ones $\langle D_g^h\rangle$, $\langle D_f^h\rangle$ and $\langle D_\gamma^h\rangle$, which are known at any scale Q from the literature. Beside the flavour index $f = u, d, c, s, b$, introduced above, we introduce a second index i running over the (r) states, the photon and the gluons $(i = g, \gamma, r)$.

The probability of generating a specific sequence of N states in the course of the evaporation of the black hole is then given by a multinomial distribution of the form

$$f(n_f, n_i, p_f, p_i) = \frac{N!}{\prod_f n_f! \prod_i n_i!} \prod_f p_f^{n_f} \prod_i p_i^{n_i} \tag{2.27}$$

which describes a typical multi-poissonian process with N trials. Notice that, to ensure proper normalization, we need to require that

$$\prod_i n_i! = n_g! n_\gamma! n_r! = n_g! n_\gamma! \left(N - \sum_f n_f - n_g - n_\gamma\right)! \tag{2.28}$$

The computation of the cumulative probabilities to produce any number of hadrons of type h by the decay of the black hole are obtained from the multinomial distribution multiplied by the fragmentation probabilities of each elementary state into (h) and summing over all possible sequences

$$\mathrm{Pr}_{\text{cum h}} \equiv \sum_{n_f, n_i} \frac{N!}{\prod_f n_f! \prod_i n_i!} \prod_f \left(p_f \langle D_f^h\rangle\right)^{n_f} \prod_i \left(p_i \langle D_i^h\rangle\right)^{n_i}. \tag{2.29}$$

A possible way to compute $\mathrm{Pr}_{\text{cum h}}$ when N is large is to multiply the multinomial distribution by a suppression factor $\mathrm{Exp}[-\Lambda(\sum_i n_i + \sum_f n_f - N)]$, with Λ a very large number, and interpret this factor as a Boltzmann weight, as in standard Monte Carlo computations of the partition function for a statistical system. Simulations can be easily done by a Metropolis algorithm and the configurations of integers selected are those for which the normalization condition $N = \sum_i n_i + \sum_f n_f$ is satisfied. In our case, since we are interested only in the mean number of hadrons produced in the decay and in their thermal spectrum, the computation simplifies if we average over all the relevant configurations.

[1] Quark and antiquark states of the same flavor have equal fragmentation functions in all hadrons

JHEP06(2005)065

3. Fragmentation and the photon component

The evolution with Q^2 of the fragmentation functions is conveniently formulated in terms of the linear combinations

$$
\begin{aligned}
D^h_\Sigma(x,Q^2) &= \sum_{i=1}^{N_F}\left(D^h_{q_i}(x,Q^2)+D^h_{\overline{q}_i}(x,Q^2)\right),\\
D^h_{(+),i}(x,Q^2) &= D^h_{q_i}(x,Q^2)+D^h_{\overline{q},i}(x,Q^2)-\frac{1}{N_F}D^h_\Sigma(x,Q^2),\\
D^h_{(-),i}(x,Q^2) &= D^h_{q_i}(x,Q^2)-D^h_{\overline{q},i}(x,Q^2),
\end{aligned}
\tag{3.1}
$$

as for these the gluon decouples from the non-singlet $(+)$ and the asymmetric $(-)$ combinations, leaving only the singlet and the gluon fragmentation functions coupled;

$$
\begin{aligned}
Q^2\frac{d}{dQ^2}D^h_{(+),i}(x,Q^2) &= \left[P_{(+)}\left(\alpha_s(Q^2)\right)\otimes D^h_{(+),i}(Q^2)\right](x),\\
Q^2\frac{d}{dQ^2}D^h_{(-),i}(x,Q^2) &= \left[P_{(-)}\left(\alpha_s(Q^2)\right)\otimes D^h_{(-),i}(Q^2)\right](x),\\
Q^2\frac{d}{dQ^2}D^h_{\Sigma}(x,Q^2) &= \left[P_{\Sigma}\left(\alpha_s(Q^2)\right)\otimes D^h_{\Sigma}(Q^2)\right](x)+\\
&\quad +2N_F\left[P_{q\to G}\left(\alpha_s(Q^2)\right)\otimes D^h_{G}(Q^2)\right](x),\\
Q^2\frac{d}{dQ^2}D^h_{G}(x,Q^2) &= \frac{1}{2N_F}\left[P_{G\to q}\left(\alpha_s(Q^2)\right)\otimes D^h_{\Sigma}(Q^2)\right](x)+\\
&\quad +\left[P_{g\to g}\left(\alpha_s(Q^2)\right)D^h_{g}(Q^2)\right](x).
\end{aligned}
\tag{3.2}
$$

The kernels that appear in the equations above are defined by

$$
\begin{aligned}
P_{(+)}\left(x,\alpha_s(Q^2)\right) &= P^V_{q\to q}\left(x,\alpha_s(Q^2)\right)+P^V_{q\to\overline{q}}\left(x,\alpha_s(Q^2)\right),\\
P_{\Sigma}\left(x,\alpha_s(Q^2)\right) &= P_{(+)}\left(x,\alpha_s(Q^2)\right)+2N_F P^S_{q\to q}\left(x,\alpha_s(Q^2)\right),\\
P_{(-)}\left(x,\alpha_s(Q^2)\right) &= P^V_{q\to q}\left(x,\alpha_s(Q^2)\right)-P^V_{q\to\overline{q}}\left(x,\alpha_s(Q^2)\right),
\end{aligned}
\tag{3.3}
$$

with $\alpha_s(Q^2)$ being the QCD fine structure constant. In the perturbative expansion of the splitting functions,

$$
P(x,\alpha_s(Q^2))=\frac{\alpha_s(Q^2)}{2\pi}P^{(0)}(x)+\left(\frac{\alpha_s(Q^2)}{2\pi}\right)^2P^{(1)}(x)+\mathcal{O}\left(\left(\frac{\alpha_s(Q^2)}{2\pi}\right)^3\right).
\tag{3.4}
$$

The timelike kernels, that we use, are given by

$$
P^{V,(0)}_{q\to q}(x) = C_F\left[\frac{3}{2}\delta(1-x)+2\left(\frac{1}{1-x}\right)_+-1-x\right],
\tag{3.5}
$$

$$
P^{V,(0)}_{q\to\overline{q}}(x) = P^{S,(0)}_{q\to q}(x)=0,
\tag{3.6}
$$

$$
P^{(0)}_{q\to G}(x) = C_F\left[\frac{1+(1-x)^2}{x}\right],
\tag{3.7}
$$

$$
P^{(0)}_{G\to q}(x) = 2N_FT_R\left[x^2+(1-x)^2\right],
\tag{3.8}
$$

$$
P^{(0)}_{G\to G}(x) = \left(\frac{11}{6}N_C-\frac{2}{3}N_FT_R\right)\delta(1-x)+2N_C\left[\left(\frac{1}{1-x}\right)_++\frac{1}{x}-2+x-x^2\right].
\tag{3.9}
$$

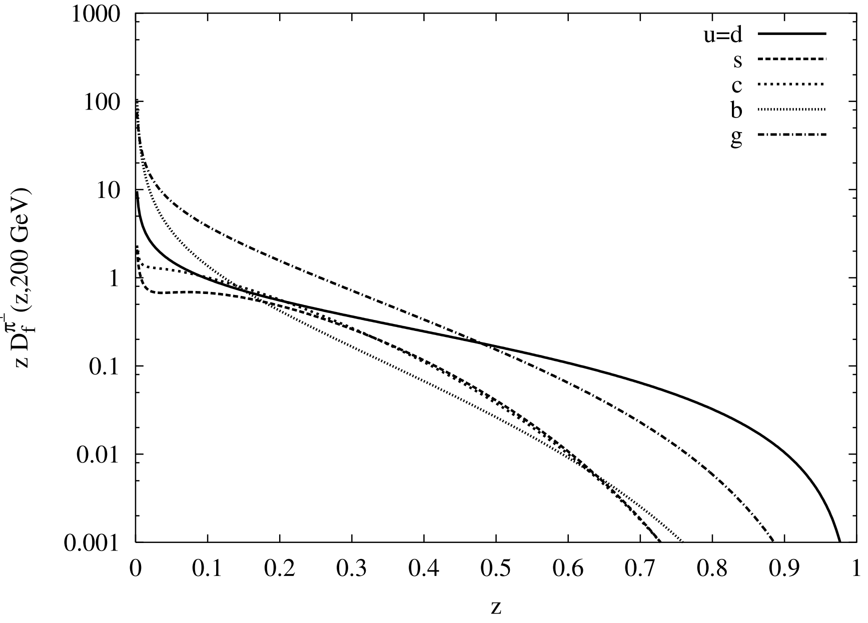

Figure 2: Fragmentation functions into $\pi^\pm$ at 200 GeV.

The formal solution of the equations is given by

$$D_a^h(x,Q^2) = D_a^h(x,Q_0^2) + \int_0^{\log\left(\frac{Q^2}{Q_0^2}\right)} d\log\left(\frac{Q^2}{Q_0^2}\right)\frac{\alpha_s(Q^2)}{2\pi}\sum_b\left[P_{a\to b}(\alpha_s(Q^2))\otimes D_b^h(Q^2)\right] \tag{3.10}$$

where Q_0 is the scale of the initial conditions $D(x,Q_0^2)$. At leading order in α_s, we solve this equation using a special ansatz

$$D_f^h(x,Q^2) = \sum_n \frac{A_n(x)}{n!}\log\left(\frac{\alpha_s(Q^2)}{\alpha_s(Q_0^2)}\right)^n \tag{3.11}$$

and generating recurrence relations at the $n+1-th$ order for the A_{n+1} coefficients in terms of the A_n [11]. It is easy to see that this corresponds to the numerical implementation of the formal solution

$$D_f^h(x,Q^2) = \mathrm{Exp}\,(tP\otimes)\,D_f^h(x,Q_0^2) \tag{3.12}$$

with $t = \alpha_s(Q^2)/\alpha_s(Q_0^2)$, where the exponential is a formal expression for an infinite iteration of convolution products. We show in figure 2 results for the fragmentation functions into pions, computed for a typical parton scale of 200 GeV. The fragmentation functions into kaons are very similar, only scaled down, roughly by a factor of 10. Analogous results for all relevant hadrons have been incorporated into our simulations.

The photon contributions to the decay of the black hole is treated separately. The evolution equation for the fragmentation functions of photons and parton fragmentation into photon $D_\gamma^\gamma(x,Q^2)$, $D_q^\gamma(x,Q^2)$ satisfy at leading order in $\alpha_{\rm em}$ and α_s (the QED and

QCD constants) the evolution equations [24]

$$\frac{\mathrm{d}D_\gamma^\gamma(x,Q^2)}{\mathrm{d}\ln Q^2} = \frac{\alpha}{2\pi} P_{\gamma\to\gamma}(x) \otimes D_\gamma^\gamma(x,Q^2) \tag{3.13}$$

which can be integrated with the initial conditions $D_\gamma^\gamma(x,Q^2) = \delta(1-x)$, and

$$\frac{\mathrm{d}D_q^\gamma(x,Q^2)}{\mathrm{d}\ln Q^2} = \frac{\alpha}{2\pi} P_{\gamma\to\gamma}(x) \otimes D_\gamma^\gamma(x,Q^2) \tag{3.14}$$

which can also be integrated with the result [25]

$$D_{\gamma/q}(x,Q^2) = \frac{\alpha}{2\pi} P_{q\to\gamma}(x) \ln\frac{Q^2}{Q_0^2} + D_q^\gamma(x,Q_0^2)\,. \tag{3.15}$$

In eq. (3.15) the second term is called the hadronic boundary conditions, which comes from an experimental fit, while the first term is the pointlike contribution and can be obtained perturbatively. A leading order fit was given in [26]

$$D_q^\gamma(x,Q_0^2) = \frac{\alpha}{2\pi}\left[-P_{q\to\gamma}(x)\ln(1-x)^2 - 13.26\right] \tag{3.16}$$

at $Q_0 = 0.14\,\mathrm{GeV}$. The kernels in these cases are given by simple modifications of the ordinary QCD kernels, for instance $P_{q\to\gamma}(x) = e_q^2/C_F P_{q\to g}(x)$ [24]. For the fragmentation functions of quarks to photons the perturbative result is given in [27].

We recall that each elementary state emitted is characterized by an average center of mass energy given by $\langle\varepsilon\rangle = M_{BH}/\langle N\rangle$.

The leptonic component $e^\pm$, $\mu^\pm$, produced by the decay, is left unaltered and provides an input for the air shower simulator as soon as these particles cross the horizon. The $\tau^\pm$s are left to decay into their main channels, while the hadronization of the u, d, s, c quarks and the gluons is treated with our code, that evolves the fragmentation functions to the energy scale $\langle\varepsilon\rangle$. The t quark is treated consistently with all its fundamental decays included; hadronization of the b quark is treated with suitable fragmentation functions and also involves a suitable evolution. As we vary M_{BH} and we scan over the spectrum of the incoming cosmic rays the procedure is repeated and rendered automatic by combining in a single algorithm all the intermediate steps. Table 1 contains the results of the renormalization group analysis of the fragmentation functions for all the partons (except the top quark) at a final scale of $Q = 200\,\mathrm{GeV}$. The initial conditions at the input scale $Q = 1.414\,\mathrm{GeV}$ for u, d, s, g, $Q = 2m_c = 2.9968\,\mathrm{GeV}$ for c and $Q = 2m_b = 9.46036\,\mathrm{GeV}$ for the b quark were taken from reference [12].

This concludes the computation of the probabilities for each hadron/lepton present in the decay products of the mini black hole. It is reasonable to assume that in the center of mass frame these particles will be produced spherically, since higher angular momenta are suppressed by the corresponding centrifugal barrier. However, the analysis of the shower profile has to be performed in the lab frame. The necessary transformation of the above initial configurations to the lab frame is given for completeness in the next section.

JHEP06(2005)065

$Q = 200\,\mathrm{GeV}$	$\pi^\pm$	π^0	$K^\pm$	$K^0/\overline{K}^0$	$p/\overline{p}$	$n/\overline{n}$
u	0.446	0.223	0.079	0.166	0.053	0.033
	0.385	0.193	0.077	0.178	0.047	0.027
d	0.446	0.223	0.166	0.079	0.033	0.053
	0.385	0.193	0.178	0.077	0.027	0.047
s	0.425	0.213	0.093	0.093	0.088	0.088
	0.295	0.147	0.077	0.077	0.070	0.070
c	0.371	0.185	0.158	0.158	0.064	0.064
	0.295	0.147	0.150	0.150	0.051	0.051
b	0.431	0.216	0.132	0.132	0.045	0.045
	0.292	0.146	0.101	0.101	0.036	0.036
g	0.428	0.214	0.135	0.135	0.044	0.044
	0.577	0.289	0.175	0.175	0.057	0.057

Table 2: For each pair of parton/hadron, the first number is the probability of fragmentation $\left(\int_{z_{\min}}^1 D_f^h(z,Q)dz\right) / \sum_{h'} \left(\int_{z_{\min}}^1 D_f^{h'}(z,Q)dz\right)$ of the parton f into the hadron h, while the second is the average energy fraction $\int_{z_{\min}}^1 zD_f^h(z,Q)dz$ of h. The energy of the parton is $Q = 200\,\mathrm{GeV}$.

4. Sphericity and boost

The transformation from the black hole frame (BHF) to the laboratory frame (LF) is performed by a Lorentz boost with speed β, the speed of the black hole in the LF. Assuming that the black hole is produced in the collision of a primary of energy E_1 in the LF and negligible mass compared to E_1, with a parton of mass M in the atmosphere, one obtains $\beta = E_1/(E_1 + M)$. A spherical distribution of a particular particle of mass m among the decay products in the BHF is transformed to an elliptical one, whose detailed form is conveniently parametrized by

$$g^* = \frac{\beta}{\beta^*} = \frac{1 - \frac{M}{E_1+M}}{\left(1 - \frac{m^2}{E^{*2}}\right)^{1/2}} \tag{4.1}$$

where $\beta^* = P^*/E^*$ is the speed of this particle in the BHF, the ratio of its BHF momentum and energy. Figure 3 depicts the relevant kinematics [28]. A particle emitted in the direction θ^* in the BHF, is seen in the direction θ in the LF, with

$$\tan\theta = \sqrt{1-\beta^2}\,\frac{\sin\theta^*}{g^* + \cos\theta^*}\,. \tag{4.2}$$

For values of $g^* \geq 1$ the shape of the 1-particle distribution in the LF is characterized by a maximum angle of emission

$$|\tan\theta_{\max}| = \sqrt{\frac{1-\beta^2}{g^{*2}-1}}\,, \tag{4.3}$$

which for $g^* = 1$ is equal to 90^o. Only for $g^* < 1$ there is backward emission in the LF.

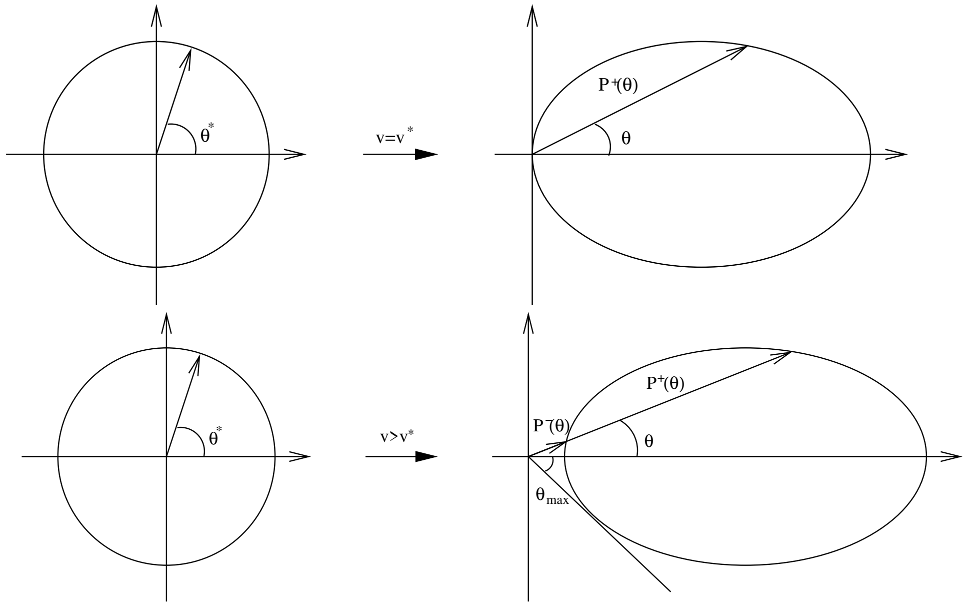

Figure 3: An s-wave distribution in the BHF is transformed in the detector frame to an elliptical one, whose detailed shape depends on the value of g^*.

As a relevant example, let us consider the case of a hadron of mass $m = 1\,\mathrm{GeV}$ and energy $E^* = 100\,\mathrm{GeV}$ emitted by a black hole, formed by an initial primary of energy $E_1 = 1000\,\mathrm{TeV}$, which hit a quark of mass $M \sim 10\mathrm{MeV}$ to form a black hole. Then $g^* = 1.00005$ and the corresponding maximum angle in the LF is $\theta_{\max} \simeq \tan\theta_{\max} = 1.4 \times 10^{-2}$, i.e. about 1 degree.

As shown in figure 3, for $g^* > 1$, relevant for our purposes, the mapping from θ^* to θ is two to one. In a given direction θ in the LF, one receives particles emitted in two different directions $\theta^{*\pm}$ in the BHF. They satisfy [28]

$$\frac{d\cos\theta^{*\pm}}{d\cos\theta} = \left(\frac{P^\pm}{P^*}\right)^2 \frac{1}{\left(\pm\cos\theta\sqrt{K}\right)} \tag{4.4}$$

where

$$K = 1 + \gamma^2(1 - g^{*2})\tan^2\theta\,, \tag{4.5}$$

and with the momenta $P^\pm$ and energies $E^\pm$ of the two branches given by

$$P^\pm = \frac{P^*\cos\theta(g^* \pm \sqrt{K})}{\gamma(1 - v^2\cos^2\theta)}\,. \tag{4.6}$$

and

$$E^\pm = \frac{m\left(\gamma^* \pm v\cos\theta\left(v^{*2}\gamma^{*2} - v^2\gamma^2\sin^2\theta\right)^{1/2}\right)}{\gamma(1 - v^2\cos^2\theta)} \tag{4.7}$$

respectively. In the above formulas $\gamma^{-1} = \sqrt{1-\beta^2}$, $v(v^*)$ is the speed of the hadron in the LF (BHF), and $(\gamma^*)^{-1} = m/E_h^* = \sqrt{1 - v^{*2}}$.

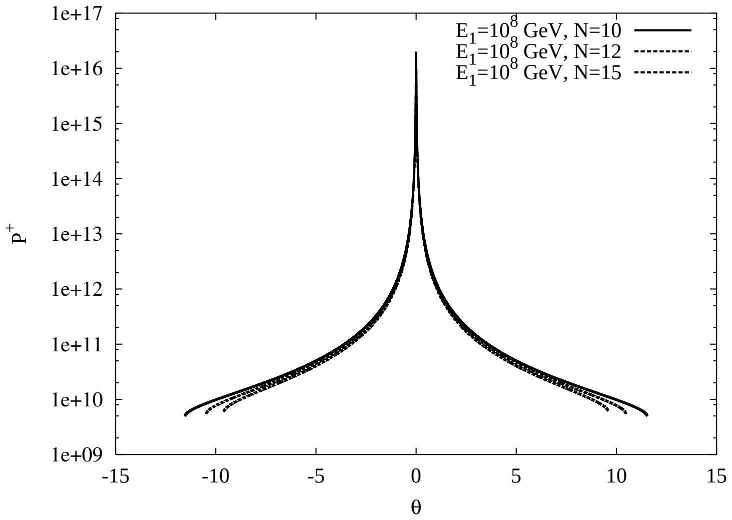

Figure 4: Plot of the P^+ branch of the momentum distribution in eV for an incoming energy of the cosmic ray $E_1 = 10^8$ GeV and for various values of N of the elementary partonic states emitted during the decay of the black hole.

The probability distribution $W_h^*(\cos\theta^*, \phi)$ of a hadron h as a function of the direction $\Omega = (\cos\theta^*, \phi)$ in the BHF, assumed spherically symmetric and normalized to the total probability Pr_h of detecting this hadron among the decay products with N elementary states, is $W_h^*(\cos\theta^*) = \mathrm{Pr}_h/2$, while the corresponding one in the LF is

$$W_h(\cos\theta) = \sum_{\pm} \frac{d\cos\theta^{*\pm}}{d\cos\theta}\, W_h^*(\cos\theta^{*\pm})\,. \tag{4.8}$$

As we have already mentioned, the structure of the partonic event (and, similarly, of the hadronic event after fragmentation) is characterized by the formation of an elliptical distribution of partons, strongly boosted toward the detector along the vertical direction. Each uniform (s-wave) distribution is strongly elongated along the arrival direction (due to the large speed of the black hole along this direction) and is characterized by two subcomponents ($W^{\pm}$), identified by a $\pm$ superscript. Their sum is the total probability distribution given in (4.8). The "+" momentum component is largely dominant and strongly peaked around the vertical direction with rather small opening angles and this behaviour can be analyzed numerically with its N dependence. In the explicit identification of the two independent distributions $\pm$ in terms of the opening angle θ, as measured in the LF, we use the relations

$$W^{\pm}(\theta) = \frac{1}{2} W^{\pm}(\cos\theta^*) \left| \frac{d\cos(\theta^*)}{d\cos\theta}^{\pm} \right| \sin\theta\,, \tag{4.9}$$

where we have introduced a factor of $1/2$ for a correct normalization of the new distribution in the θ variable. Figure 4 illustrates an example of the component P^+ as a function of θ for $E_1 = 10^5$ TeV. Almost all final momentum is emitted inside a cone of angle 5 degrees. Very similar is the behaviour of the probability distribution W^+, while W^- and P^- are negligible at these energies, compared to W^+ and P^+, respectively.

5. Air shower simulations

The simulation of the events is performed at the last stage, using an air shower simulator. We have used CORSIKA [8] with appropriate initial conditions on the spectrum of the incoming particles in order to generate the full event measured at detector level. We have performed two separate sets of simulations. The first set being the signal events, i.e. the showers produced by an evaporating mini black hole, created at some altitude with a given speed. The second set consists of the benchmark "normal" events, the showers resulting from a proton-air initial collision with the same energy and at the same height. The difference between the first and the second set is, of course, attributed to the difference in the final states prior to the development of the air showers. In most of the simulations we have assumed that the black hole creation takes place in the lower part of the atmosphere, not far from the level of the detector and at a varying altitude X_0. The reason is that, as mentioned in the introduction, one of our interests is the investigation of the possibility that the Centauro events may be related to evaporating mini black holes, formed by the collision of weakly interacting particles (e.g. neutrinos) which penetrate the atmosphere. Of course, for generality and completeness we have simulated events happening at higher altitudes as well.

The overall shower, defined as the superposition of the various sub-components, develops according to an obvious cylindrical symmetry around the vertical z-axis near the center. In the simulations we take the shower direction to be at zero zenith with respect to the plane of the detector. This is no harm to generality, because the multiplicities, the lateral distributions and the electromagnetic to hadronic ratio we shall mainly concentrate on, do not depend on the direction of the shower. We have kept the gravity scale M_* constant at 1 TeV and varied the mass of the black hole according to the available center of mass energy E. As we have already discussed in the previous sections, as a benchmark process we have selected a proton-air impact at the same X_0 with the boundary condition

$$N_p(E, X_0) = \mathrm{Pr}_p \delta \left(E - \frac{M_{BH}}{f_n} \right) \tag{5.1}$$

which occurs with probability 1 ($\mathrm{Pr}_p = 1$).

We are interested both in the behaviour of the multiplicities and in the lateral distributions of the cascades developed at detector level as functions of the energy E. For this purpose we have defined the opening of the conical shower after integration over the azimuthal angle, as in [29], and given the symmetry of the event, we plot only the distance from the center as a relevant parameter of the conical shower.

A varying number of extra dimensions $n = 0, 1, \ldots, 4$ implies a different ratio for bulk-to-brane energy emission, a different average number of elementary decaying states and different energy distributions among these. We have varied the LF energy E_1 of the primary, thereby varying the mass of the black hole resonance, in the interval $10^{15} - 10^{20}$ eV. The hadronization part of our code has been done by changing the $\mathrm{Pr}_h(E)$ obtained from a numerical solution of the fragmentation functions separately for each value of the energy shared.

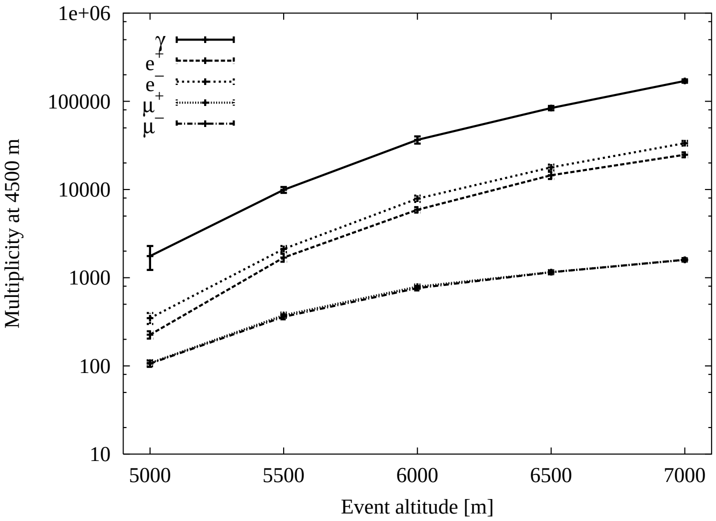

Figure 5: Benchmark event: multiplicities of photons, $e^{\pm}$, $\mu^{\pm}$ at an observation level of 4500 m as a function of the altitude of the first impact. The multiplicities observed at 5000 m show similar behaviour, reduced by roughly a factor of 2.

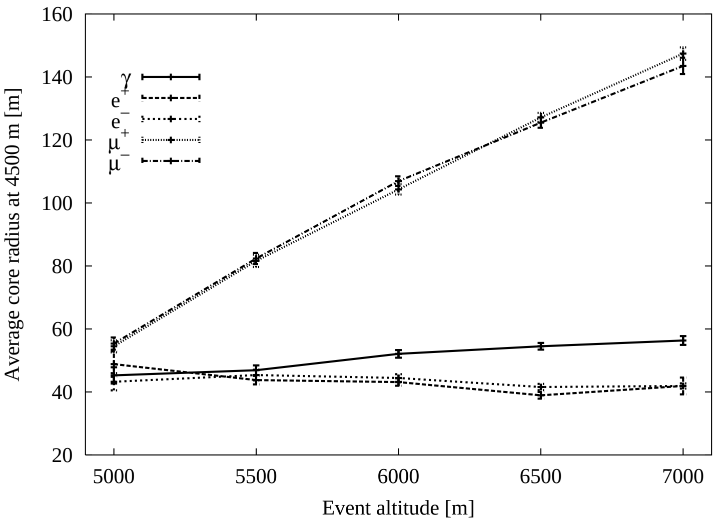

Figure 6: Average radial opening of the shower of photons, $e^{\pm}$, $\mu^{\pm}$ at an observation level of 4500 m as a function of the altitude of proton's first interaction. The radial opening of the showers at 5000 m is qualitatively identical, with a slight increase in the slopes of the muon curves.

- *Characteristics of the benchmark events*

  We start with the numerical study of the partial and total multiplicities of the various sub-components and of their lateral distributions in the benchmark event, representative of the normal ultra high energy cosmic ray events. The results for photons and leptons are shown in figures 5 to 6 as functions of the altitude of the impact and for two different observation points at 4,500 m and 5,000 m, approximately the altitudes of the detectors at Pamir and Chacaltaya, respectively. These preliminary plots, based on actual simulations of a proton-to-air nucleus impact at 10^{15} eV, not surprisingly show a steady growth of the multiplicities of the secondaries as we raise the point of first impact above the detector.

The statistical errors in the simulations (80 uncorrelated events have been collected per point) are rather small, quite uniformly over all the altitudes of the impact, and indicate a satisfactory stability of the result. The positions of the detectors do not seem to have an appreciable impact on the characteristics of the secondaries. As for the lateral distributions we observe an increase with the event altitude, mainly in the opening of the muonic component of the showers. Its slope is larger roughly by 15% at 5000 m. For the photons and even more so for the electrons and positrons the openings stay almost constant. Also in this case the statistical fluctuations are rather small. On the basis of these results we have selected for the remaining simulations a first impact at 5,500 m and the observation (detector) level at 5,000 m. However, for comparison, we will also show later results of a second set of simulations that have been performed with the first impact at 15,000 m.

- *Multiplicities in black hole mediated events*

For the multiplicities themselves the situation is much cleaner. In figure 7 we show the behaviour of the total multiplicities in black hole mediated events and in standard events, as functions of the energy and for a varying number of extra dimensions.

Notice that for the lower energies in the plot the total multiplicities of the black hole mediated events may be smaller than 100 and certainly much smaller than in normal events. Incidentally, this is consistent with the Centauros.

We do not plot here the corresponding curves for each species of final particles separately [30]. They all show the same behaviour as the total multiplicities. The normal events start always with, roughly, one order of magnitude more particles of each species in the low energy part of the plot and end up with fewer particles in the high energy part of the plot. All these curves are very well fitted in a log-log plot by a linear relation of the form

$$N = 10^{q(n)} E_1^{\sigma(n)} \tag{5.2}$$

with intercepts $q(n)$ and slopes $\sigma(n)$, that increase with the number of extra dimensions n. In figure (a) the slopes of the benchmark events are smaller than those of the black hole events and show a larger intercept. This feature is common to all the sub-components of the air showers. This may be traced back to figure 1, according to which at low energies the number of particles from the black hole decay is much smaller than the ones produced in a normal interaction. However, it increases rapidly with energy and leads to larger numbers of final particles in the showers, in the high energy parts of the multiplicity plots.

As we increase the altitude of the first impact, in plots of type (b) we find a similar trend, but the differences in the total and partial multiplicities are much harder to discern for black holes and standard events. This is expected, since for collisions

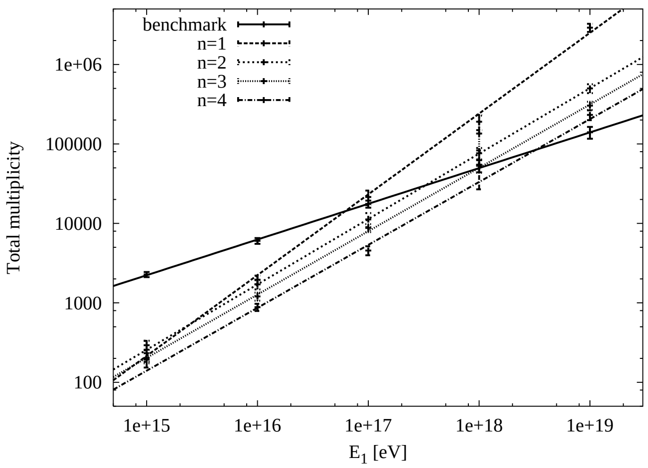

(a)

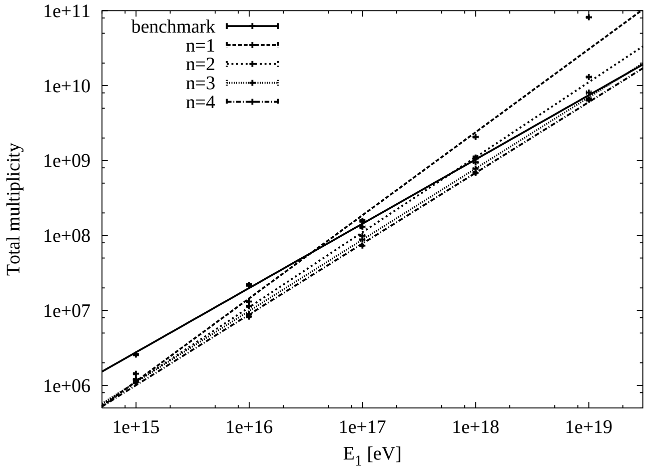

(b)

Figure 7: Plot of the total particle multiplicity as a function of E_1. Case (a) is for a first impact at 5,500 m, while (b) at 15,000 m.

starting at higher altitudes the showers are all fully developed and the differences between the two underlying events are less pronounced.

Another feature of the black hole events is that the slopes and the intercepts of the various multiplicity plots, for a given choice of the altitude of the initial impact, are linearly correlated. To illustrate this point, we refer to figure 8 from which this behaviour is immediately evident. To generate these figures for the total multiplicities (shown here) or for the partial multiplicities (not shown), we have plotted the parameters (σ, q) of the corresponding multiplicity plot for all values of the number of extra dimensions. The results shown, clearly indicate that the relation between the intercept q and the slope σ appearing in equation (5.2) is linear and independent of

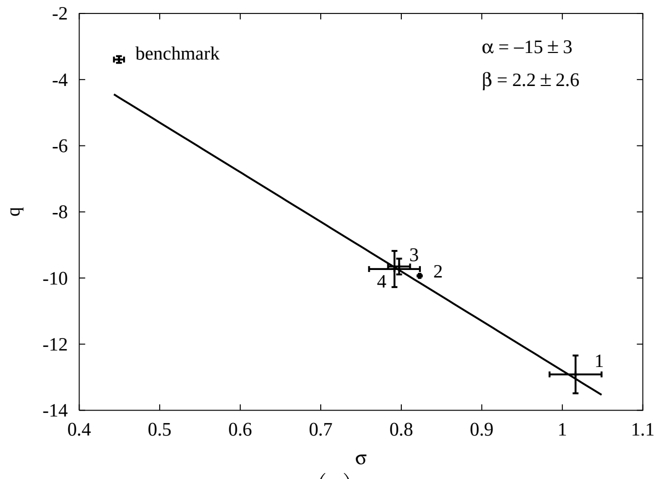

(a)

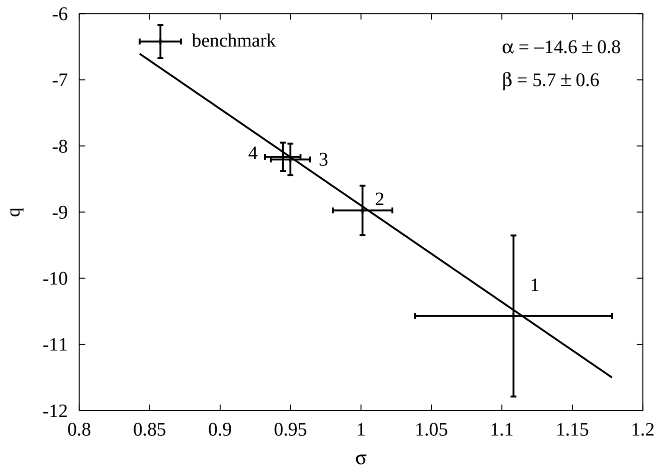

(b)

Figure 8: Parameter fit for the intercepts and the slopes of the curves in figure 7 for the total multiplicities. The numbers over each point in this plot indicate the value of the extra-dimensions. The (σ, q) parameters are fitted to a straight line $q = \alpha\,\sigma + \beta$ independently of the numbers of extra dimensions. (a) is the fit for 5,500 m, (b) for 15,000 m. The benchmark is also shown in the plot, but has not been used in the fit.

n, i.e.

$$q = \alpha\,\sigma + \beta \tag{5.3}$$

with α and β typical of a given setup (photons, total multiplicities, etc.) but insensitive to the parameter n. Therefore, black hole events are characterized by particle multiplicities at the detector of the generic form

$$N = 10^{\alpha\,\sigma + \beta} E_1^{\sigma}\,. \tag{5.4}$$

- *Lateral distributions in black hole mediated events*

Figure 9 presents, as an example, the results of our study of the lateral distribution of the photons in the shower as a function of the incoming energy E_1. The behaviour of leptons, pions or other hadrons is the same, for both altitudes of the initial impact studied here. The average opening of the shower as measured at detector level is plotted versus energy in a log-log scale. Notice a growing opening of the shower as we raise the energy of the black hole resonance, which is more remarked for a lower number of extra dimensions. In contrast, the benchmark simulation shows a slight decrease with energy. The larger opening of the shower in black hole mediated events - compared to standard air showers - is due to the s-wave emission typical of a black hole decay, which is very different from an ordinary collision. In contrast to the case of multiplicities, here simulations of type (a) and (b) show a similar trend, with very distinct features between standard and black hole mediated events. Notice, that in this case the difference in the partonic content of the two kinds of events is less relevant, since it is the geometrical fireball emission in the black hole case, which is responsible for the generation of larger lateral distributions.

Also in this case we discover a linear relation between the average radius R of the conical openings and energy, relation that can be fitted to a simple power law

$$R = 10^{q'(n)} E_1^{\sigma'(n)} . \tag{5.5}$$

In analogy to what was done in figure 8, one may plot q' versus σ' for the various straight lines of figure 9, or of analogous plots for other components of the showers. There seems to be always a linear relation between slopes and intercepts of equation (5.5)

$$q' = \alpha' \sigma' + \beta' \tag{5.6}$$

with α' and β' typical for a given particle species and altitude of initial impact, but again independent of n. For example, for the case of photons and first impact at 15000 m one obtains $\alpha' = -11.31 \pm 0.02$ and $\beta' = -0.29 \pm 0.02$.

6. Discussion

A rather detailed analysis was presented of certain observables which characterize the air showers formed, when a high energy collision in the atmosphere leads to the intermediate formation of a mini black hole. We focused our attention on the particle partial and total multiplicities in these events and on the geometrical opening of the showers produced, as functions of the entire ultra high energy spectrum of the incoming primary source. We have shown that in a double logarithmic scale the energy versus multiplicity as well as the energy versus shower-size plots are linear, characterized by slopes which depend on the number of extra dimensions. We have compared these predictions with standard (benchmark) simulations and corrected for the energy which escaped in the bulk, or was emitted by the black holes at stages prior to the Schwarzschild phase. Black hole events are characterized by faster growing multiplicities for impacts taking place close to the detector; impacts at higher altitudes share a similar trend, but less pronounced. The multiplicities

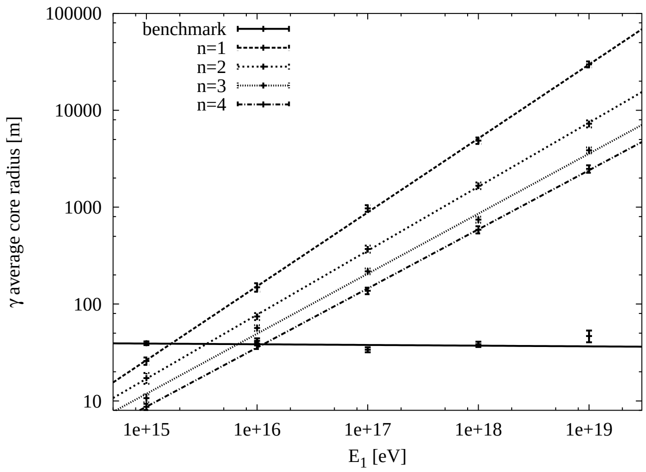

(a)

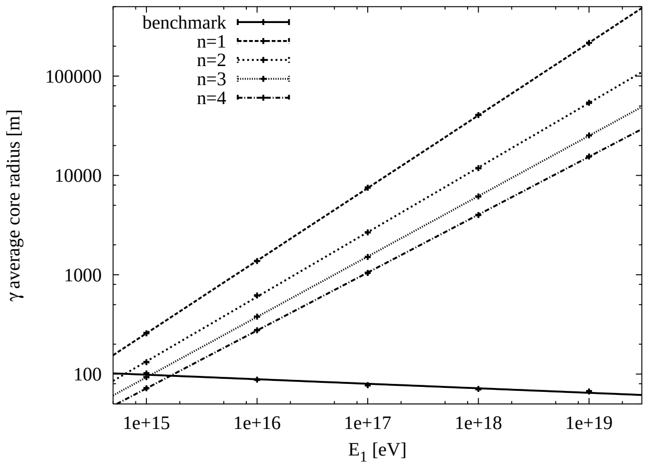

(b)

Figure 9: Plot of the average radius R of the core of the shower of photons as a function of E_1 for a black hole with a varying number of extra dimensions. The benchmark result is also shown for comparison. (a) 5,500 m, (b) 15,000 m.

JHEP06(2005)065

from the black hole are much smaller in the lower part of the energy range, while they become larger for higher energies. The lateral distributions appear to be the most striking signature of a black hole event. Due to the higher p_Ts involved, they are much larger than in the benchmark standard simulations.

Our analysis can be easily generalized to more complex geometrical situations, where a slanted entry of the original primary is considered and, in particular, to horizontal air showers, which are relevant for the detection of neutrino induced showers, on which we hope to return in a future work.

As a byproduct, our results seem to offer considerable support to the black hole interpretation of the Centauro events. As was observed in [5] their energy threshold is naturally accomodated in the context of TeV scale gravity with large extra dimensions. Also, the number of events is consistent with the available knowledge of the ultra high energy neutrino flux and the geometric cross section for black hole production in neutrino nucleon collisions. From the present work we learn that the total multiplicities are close to the ones observed. The multiplicities in showers which originate at even lower altitudes, as is presumably the case for the Centauro events, will be smaller and, based on the above graphs, will be in perfect agreement with the observed values.

We would like to mention that in addition to the above, we also studied the crucial ratio $E_{\text{hadron}}/E_{\text{em}}$, which is anomalously large in the Centauro events. Unfortunately, our simulations showed wild fluctuations of this ratio and we could not draw a definite conclusion. Superficially, though, there does not seem to be a statistically significant difference in this observable, between the benchmark events and the black hole mediated ones. This is against the black hole interpretation of the Centauros. However, it is conceivable that starting at lower altitudes this ratio will be improved, since the kaons produced by the black hole's "democratic" evaporation will not have enough time to decay and will be counted as hadrons. Similarly, if a DCC forms as a result of the decay of the black hole, the prediction for the ratio of the hadronic to the electromagnetic component is expected to increase drastically.

Needless to say, the subject of black hole production and evaporation touches upon several different subfields of theoretical and experimental high energy physics and astrophysics. A partial list includes the fields of cosmic ray physics and of the air shower formation in the atmosphere, of quantum gravity/string theory, of non-perturbative low energy QCD and of the physics of the quark-gluon plasma. Here we made a first naive step, but given the incomplete understanding of all of these, it is clear that a lot more has to be done, both in theory and experiment, before one can safely and reliably confront the observational data.

Acknowledgments

We thank Andrei Mironov, Alexey Morozov, Raf Guedens, Dominic Clancy and Greg Landsberg for helpful discussions. The work of T.N.T. is partially supported by the grants HRPN-CT-2000-00122 and MRTN-CT-2004-512194 from the EU, as well by the Hellenic Ministry of Education grants "O.P.Education - Pythagoras" and "O.P.Education - Heraklitos". The work of C.C. and A.C. is supported by INFN of Italy (BA21). The simulations have been performed at the INFN-Lecce computer cluster. C.C. thanks the Theory Group at the University of Crete and in particular E. Kiritsis for hospitality, and the Theory Division at the Max Planck Institute in Munich for hospitality while completing this work.

References

[1] N. Arkani-Hamed, S. Dimopoulos and G.R. Dvali, *The hierarchy problem and new dimensions at a millimeter*, *Phys. Lett.* **B 429** (1998) 263 [hep-ph/9803315];
I. Antoniadis, N. Arkani-Hamed, S. Dimopoulos and G.R. Dvali, *New dimensions at a millimeter to a fermi and superstrings at a TeV*, *Phys. Lett.* **B 436** (1998) 257 [hep-ph/9804398];

L. Randall and R. Sundrum, *A large mass hierarchy from a small extra dimension*, *Phys. Rev. Lett.* **83** (1999) 3370 [hep-ph/9905221];
L. Randall and R. Sundrum, *An alternative to compactification*, *Phys. Rev. Lett.* **83** (1999) 4690 [hep-th/9906064].

[2] S. Dimopoulos and G. Landsberg, *Black holes at the LHC*, *Phys. Rev. Lett.* **87** (2001) 161602 [hep-ph/0106295].

[3] A partial list on black hole formation at TeV energies includes S.B. Giddings and S. Thomas, *High energy colliders as black hole factories: the end of short distance physics*, *Phys. Rev.* **D 65** (2002) 056010 [hep-ph/0106219];
J.L. Feng and A.D. Shapere, *Black hole production by cosmic rays*, *Phys. Rev. Lett.* **88** (2002) 021303 [hep-ph/0109106];
G. Landsberg, *Discovering new physics in the decays of black holes*, *Phys. Rev. Lett.* **88** (2002) 181801 [hep-ph/0112061];
S.I. Dutta, M.H. Reno and I. Sarcevic, *On black hole detection with the OWL/Airwatch telescope*, *Phys. Rev.* **D 66** (2002) 033002 [hep-ph/0204218];
K. Cheung, *Black hole, string ball and p-brane production at hadronic supercolliders*, *Phys. Rev.* **D 66** (2002) 036007 [hep-ph/0205033];
A. Chamblin and G.C. Nayak, *Black hole production at LHC: string balls and black holes from p p and lead lead collisions*, *Phys. Rev.* **D 66** (2002) 091901 [hep-ph/0206060];
A. Ringwald and H. Tu, *Collider versus cosmic ray sensitivity to black hole production*, *Phys. Lett.* **B 525** (2002) 135 [hep-ph/0111042];
M. Kowalski, A. Ringwald and H. Tu, *Black holes at neutrino telescopes*, *Phys. Lett.* **B 529** (2002) 1 [hep-ph/0201139];
M. Bleicher, S. Hofmann, S. Hossenfelder and H. Stocker, *Black hole production in large extra dimensions at the Tevatron: new limit on the fundamental scale of gravity*, *Phys. Lett.* **B 548** (2002) 73 [hep-ph/0112186];
L. Anchordoqui and H. Goldberg, *Experimental signature for black hole production in neutrino air showers*, *Phys. Rev.* **D 65** (2002) 047502 [hep-ph/0109242];
L.A. Anchordoqui, J.L. Feng, H. Goldberg and A.D. Shapere, *Black holes from cosmic rays: probes of extra dimensions and new limits on TeV-scale gravity*, *Phys. Rev.* **D 65** (2002) 124027 [hep-ph/0112247];
Y. Uehara, *Production and detection of black holes at neutrino array*, *Prog. Theor. Phys.* **107** (2002) 621 [hep-ph/0110382];
J. Alvarez-Muniz, J.L. Feng, F. Halzen, T. Han and D. Hooper, *Detecting microscopic black holes with neutrino telescopes*, *Phys. Rev.* **D 65** (2002) 124015 [hep-ph/0202081];
K. Cheung, *Black hole production and large extra dimensions*, *Phys. Rev. Lett.* **88** (2002) 221602 [hep-ph/0110163];
P. Kanti and J. March-Russell, *Calculable corrections to brane black hole decay, II. Greybody factors for spin 1/2 and 1*, *Phys. Rev.* **D 67** (2003) 104019 [hep-ph/0212199];
I. Mocioiu, Y. Nara and I. Sarcevic, *Hadrons as signature of black hole production at the LHC*, *Phys. Lett.* **B 557** (2003) 87 [hep-ph/0301073].

[4] S.B. Giddings, *Black hole production in TeV-scale gravity and the future of high energy physics*, *eConf* **C010630** (2001) P328 [hep-ph/0110127].

[5] A. Mironov, A. Morozov and T.N. Tomaras, *Can centauros or chirons be the first observations of evaporating mini black holes?*, hep-ph/0311318, to appear in ZhETF.

[6] T.N. Tomaras, *Centauros and/or chirons as evaporating mini black holes*, contribution to the proceedings of the XIII ISVHECRI, Pylos, September 2004 [hep-ph/0411081].

[7] E. Gladysz-Dziadús, *Are centauros exotic signals of the QGP?*, *Phys. Part. Nucl.* **34** (2003) 285 [hep-ph/0111163].

[8] D. Heck, J. Knapp, J.N. Capdevielle, G. Schatz and T. Thouw, *CORSIKA: a Monte Carlo code to simulate extensive air showers*, *FZKA* (1998) 6019.

[9] N.N. Kalmykov, S.S. Ostapchenko, A.I. Pavlov, *Quark-gluon string model and EAS simulation problems at ultra-high energies*, *Nucl. Phys.* **52** *(Proc. Suppl.)* (1997) 17.

[10] R.S. Fletcher, T.K. Gaisser, P. Lipari and T. Stanev, *SIBYLL: an event generator for simulation of high-energy cosmic ray cascades*, *Phys. Rev.* **D 50** (1994) 5710.

[11] A. Cafarella and C. Corianò, *Direct solution of renormalization group equations of QCD in x space: NLO implementations at leading twis*, *Comput. Phys. Commun.* **160** (2004) 213 [hep-ph/0311313].

[12] B.A. Kniehl, G. Kramer and B. Potter, *Fragmentation functions for pions, kaons and protons at next-to-leading order*, *Nucl. Phys.* **B 582** (2000) 514 [hep-ph/0010289]; *Testing the universality of fragmentation functions*, *Nucl. Phys.* **B 597** (2001) 337 [hep-ph/0011155].

[13] P. Kanti, *Black holes in theories with large extra dimensions: a review*, *Int. J. Mod. Phys.* **A 19** (2004) 4899 [hep-ph/0402168].

[14] M.B. Voloshin, *Semiclassical suppression of black hole production in particle collisions*, *Phys. Lett.* **B 518** (2001) 137 [hep-ph/0107119]; *More remarks on suppression of large black hole production in particle collisions*, *Phys. Lett.* **B 524** (2002) 376 [hep-ph/0111099].

[15] S.W. Hawking, *Particle creation by black holes*, *Commun. Math. Phys.* **43** (1975) 199.

[16] R.C. Myers and M.J. Perry, *Black holes in higher dimensional space-times*, *Ann. Phys. (NY)* **172** (1986) 304.

[17] N. Sanchez, *Absorption and emission spectra of a Schwarzschild black hole*, *Phys. Rev.* **D 18** (1978) 1030.

[18] R. Emparan, G.T. Horowitz and R.C. Myers, *Black holes radiate mainly on the brane*, *Phys. Rev. Lett.* **85** (2000) 499 [hep-th/0003118].

[19] D.N. Page, *Particle emission rates from a black hole: massless particles from an uncharged, nonrotating hole*, *Phys. Rev.* **D 13** (1976) 198.

[20] M. Cavaglià and S. Das, *How classical are TeV-scale black holes?*, *Class. and Quant. Grav.* **21** (2004) 4511 [hep-th/0404050];
R. Casadio and B. Harms, *Can black holes and naked singularities be detected in accelerators?*, *Int. J. Mod. Phys.* **A 17** (2002) 4635 [hep-th/0110255].

[21] M. Cavaglià, *Black hole multiplicity at particle colliders (do black holes radiate mainly on the brane?)*, *Phys. Lett.* **B 569** (2003) 7 [hep-ph/0305256].

[22] E.-J. Ahn, M. Ave, M. Cavaglià and A.V. Olinto, *TeV black hole fragmentation and detectability in extensive air-showers*, *Phys. Rev.* **D 68** (2003) 043004 [hep-ph/0306008].

[23] D.M. Eardley and S.B. Giddings, *Classical black hole production in high-energy collisions*, *Phys. Rev.* **D 66** (2002) 044011 [gr-qc/0201034].

[24] See M. Klasen, *Theory of hard photoproduction*, *Rev. Mod. Phys.* **74** (2002) 1221 [hep-ph/0206169], and references therein.

JHEP06(2005)065

[25] A. Gehrmann-De Ridder, T. Gehrmann and E.W.N. Glover, *Radiative corrections to the photon + 1jet rate at LEP*, *Phys. Lett.* **B 414** (1997) 354 [hep-ph/9705305].

[26] ALEPH collaboration, D. Buskulic et al., *First measurement of the quark to photon fragmentation function*, *Z. Physik* **C 69** (1996) 365.

[27] J. Qiu and X. Zhang, *Virtual photon fragmentation functions*, *Phys. Rev.* **D 64** (2001) 074007 [hep-ph/0101004];
E. Braaten and J. Lee, *Fragmentation functions for lepton pairs*, *Phys. Rev.* **D 65** (2002) 034005 [hep-ph/0102130].

[28] E. Byckling and K. Kajantie, *Particle kinematics*, Wiley, 1972.

[29] A. Cafarella, C. Corianò and A.E. Faraggi, *Large scale air shower simulations and the search for new physics at Auger*, *Int. J. Mod. Phys.* **A 19** (2004) 3729 [hep-ph/0308169].

[30] More graphs and other important details may be found in the first version of A. Cafarella, C. Corianò and T.N. Tomaras, *Cosmic ray signals from mini black holes in models with extra dimensions: an analytical/Monte Carlo study*, hep-ph/0410358.

JHEP06(2005)065